World Journal of Engineering and Technology, 2022, 10, 241-253
https://www.scirp.org/journal/wjet
ISSN Online: 2331-4249
ISSN Print: 2331-4222

Laser Beam Welding of 600 MPa Quenched and Tempered High-Strength Steel

Pritchard Elmon Marozva[1*], Bruno Roberts Mose[2], Abdel-Monem El-Batahgy[3], Thomas Ochuku Mbuya[4]

[1]Department of Mechanical Engineering, Pan African University Institute for Basic Sciences, Technology and Innovation, Nairobi, Kenya
[2]Department of Mechanical Engineering, Jomo Kenyatta University of Agriculture and Technology, Nairobi, Kenya
[3]Manufacturing Technology Department, Central Metallurgical Research and Development Institute (CMRDI), Cairo, Egypt
[4]Department of Mechanical & Manufacturing Engineering, University of Nairobi, Nairobi, Kenya
Email: *pritchardmarozva@yahoo.com

How to cite this paper: Marozva, P.E., Mose, B.R., El-Batahgy, A.-M. and Mbuya, T.O. (2022) Laser Beam Welding of 600 MPa Quenched and Tempered High-Strength Steel. *World Journal of Engineering and Technology*, **10**, 241-253.
https://doi.org/10.4236/wjet.2022.102015

Received: March 1, 2022
Accepted: May 8, 2022
Published: May 11, 2022

Abstract

Conventional fusion arc welding of high-strength quenched and tempered steel can be improved through the use of non-conventional laser beam welding. This article presents the investigations of autogenous bead on plate and butt CO_2 Laser Welding (LW) of 7 mm thick high-strength quenched and tempered low alloy SM570 (JIS) steel plates. The influence of laser welding parameters, mainly welding speed, defocusing distance and shielding gas flow rate on the weld profile, *i.e.*, weld zone penetration depth and width, microstructure and mechanical properties of welded joints was determined. All welded joints showed smooth and uniform weld beads free from superficial porosity and undercuts. The selected best welding conditions were a laser power of 5.0 kW, welding speed of 500 mm/min, argon gas shielding flow rate of 30 L/min and a defocusing distance of −0.5 mm. It was observed that these conditions gave complete penetration and minimized the width of the weld bead. The microstructure of the welded joints was evaluated by light optical microscopy. The weld metal (WM) and heat-affected zone (HAZ) near weld metal achieved maximum hardness (355 HV). The tensile fractured samples showed the ductile mode of failure and ultimate tensile strength of 580 MPa.

Keywords

Laser Welding, High-Strength Steel, Quenched and Tempered, Bead on Plate Joint, Butt Joint, Heat-Affected Zone (HAZ), CO_2 Autogenous Laser Welding, Mechanical Properties

1. Introduction

Quenched and tempered high-strength steels are desirable for use in many industrial applications because they contain low carbon composition and preferable thermomechanical properties. High-strength quenched and tempered low alloy steels derive their strength from quenching, a process by which the steel is rapidly cooled to room temperature and temper heat treatment where the steel is heated to a temperature well below the melting point at a suitable rate, to increase the steel ductility, toughness and the grain size of the matrix. The quenching and tempering processes produce a microstructure largely made up of tempered martensite with little amounts of lower bainite [1] [2] [3].

These steels have the capability to meet the demand for higher-strength construction grade material. Due to their ability to protect products from environmental degradation, their reduced weight, high-strength and high impact values, quenched and tempered high-strength steels are widely used in the construction of numerous critical applications including bridges, ships, large-scale petroleum storage tanks and containers [4] [5] [6].

The welding of high-strength steels has had major drawbacks such as cold cracking, residual stresses and distortion where conventional fusion arc welding processes such as SMAW, GMAW, SAW have been employed [7] [8] [9] [10] [11] and in most cases, precautions such as preheating and post-weld heat treatment (PWHT) are employed [12] [13] [14] [15] [16]. These treatments are however costly and associated with some hazards. To maintain the mechanical properties as well as minimize distortion of arc welded joints which are a great challenge because of the associated high heat input, there is a need to explore new solutions in the production process on improving the weldability of these steels. The use of high energy density and low heat input process in Laser Beam Welding ensures narrow welds, a smaller heat-affected zone (HAZ), which cools very rapidly with very little distortion, and a high depth-to-width ratio [17] [18] [19] [20]. Previous investigations have demonstrated that the weld metal's microstructure and the HAZ of steel are influenced by the welding speed, defocusing distance, and shielding gas flow rate [21]-[27]. In addition, the stability of the keyhole and the escape of hydrogen in the molten pool are largely influenced by defocusing distance and gas shielding which often leads to the formation of undesired porosities during welding [28] [29] [30]. Inevitably, it is expected that the microstructure and the mechanical properties of welded joints of high-strength quenched and tempered low alloy SM570 (JIS) steel are affected by the welding process parameters.

To achieve the best product quality and high production rates, the present work was conducted to explore the effect of laser power, welding speed, defocusing distance and shielding gas flow rate on the microstructure and mechanical properties of welded joints of quenched and tempered high-strength steel. Since welding is widely used in the fabrication of various engineering components, understanding the factors affecting the quality of welded joints is critical

for maintaining their mechanical properties.

2. Experimental Procedure

The 7.0 mm thick plates of SM570 low alloy high-strength steel with the highest strength and toughness among the steel grades under JIS G3106 welded structure steel, were chosen for laser welding experiments. Their chemical composition and mechanical properties are given in Table 1 and Table 2 respectively.

Both bead-on-plate (Figure 1) and autogenous square butt-welded joints (Figure 2) were produced using a CO_2 laser system with 5 kW maximum output power (CW) and a CNC welding head. Figure 2 shows a schematic illustration of the butt joints of 7 mm thickness. The steel plates were machined to geometry of 150 mm × 100 mm × 7 mm and then welded perpendicular to the rolling direction.

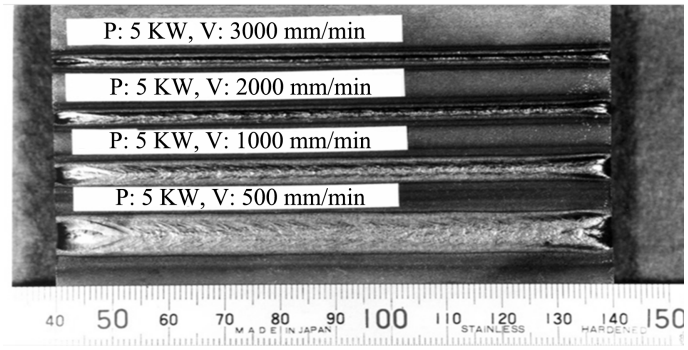

Figure 1. BOP image of the welded JIS G3106 SM570 plate.

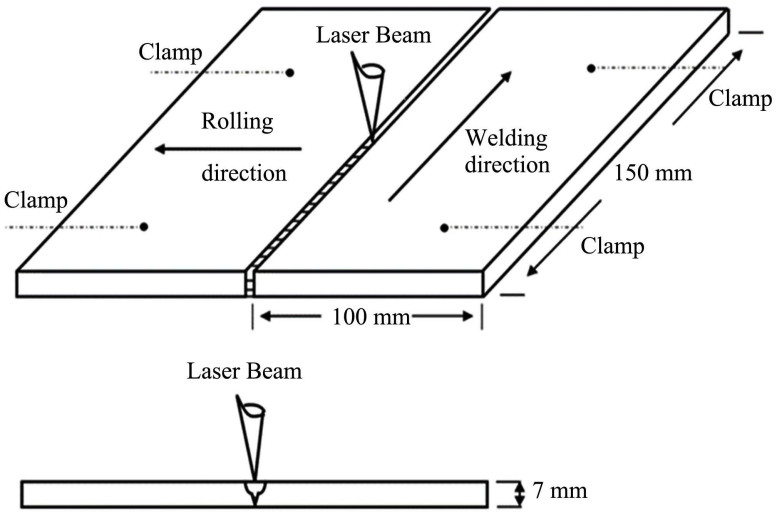

Figure 2. Experimental setup of laser beam welding.

Table 1. Chemical composition (wt%) of the used base metal.

Base metal	C	Mn	Si	S	P
JISG3106 SM570	0.18	1.60	0.55	0.035	0.035

Table 2. Mechanical properties of the used base metal.

YS (N/mm^2)	UTS (N/mm^2)	Elong (%)	Charpy absorbed energy-5 C (J)
460 min	570 - 720	26 min	47 min

Table 3 shows the investigated laser welding parameters were laser power (P), welding speed (S), defocusing distance (Dd), and shielding gas flow rate. At a constant laser power of 5.0 kW, the welding speed varied between 0.5 and 3.0 m/min, the defocusing distance varied between 0.0 mm and 1.0 mm. To protect the weld bead from contamination and to reduce the formation of absorbing plasma, argon gas shielded both the weld pool top and bottom at a flow rate between 15 and 30 L/min.

Visual examinations of laser beam welded joints showed neither internal nor external welding defects. Then, various specimens were cut in the cross-sections of the welds and prepared through grinding with grinding papers of various grit sizing from coarse to fine in the order 120, 240, 320, 600, 800 and 1000 and surface polishing with alumina paste. Natal solution was used for etching 2% Nitric acid (HNO_3) and 98% Alcohol (CH_3OH). A low-magnification stereoscope was used to determine the weld structure and an optical microscope was used for microstructure analysis. To investigate the hardness distributions through the weld, heat-affected zone and base metal, microhardness was measured at a load of 300 g by a Vickers testing machine (Matsuzawa, Akita, Japan). Tensile testing was performed by a universal tensile testing machine (Sinofound CO., Beijing China) integrated with computerized control and data acquisition system. Flat tensile specimens were prepared from the laser beam butt welds (Figure 3(a)) according to ASTM A370 [31]. Impact test specimens were prepared by etching (2% nital) to indicate the weld metal (WM), HAZ and the base metal (BM). A flaw or notch was introduced on the impact test specimens in the 3 different weld zones in order to examine the weld toughness at these locations (Figure 3(b)). The amount of energy absorbed by the material during fracture was determined at −20˚C.

3. Results and Discussions

3.1. Macrostructure Investigation

3.1.1. Effect of Welding Speed

The influence of welding speed on the weld profile was investigated at the selected laser power (5 kW) and a defocusing distance of −0.5 mm. Initial results of the bead-on-plate laser welding showed incomplete penetration for the 10 mm thickness with variations in welding speed from 3 to 0.5 m/min, Figure 4.

However complete penetration was achieved on the 7 mm thickness (see Figure 5). Figure 6 shows the relationship between welding speed and fusion zone depth/width ratio. Increasing the welding speed from 0.6 to 1 m/min results in a sharp increase in the depth/width ratio from 1.23 to 1.38.

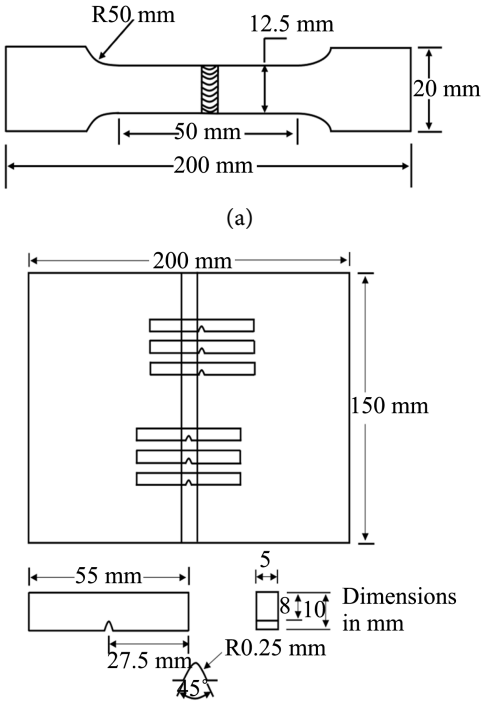

Figure 3. Schematic illustration and dimensions of (a) transverse tensile test specimen of the welded joint, (b) V-notch location of the impact test specimen in the BM, HAZ and WM.

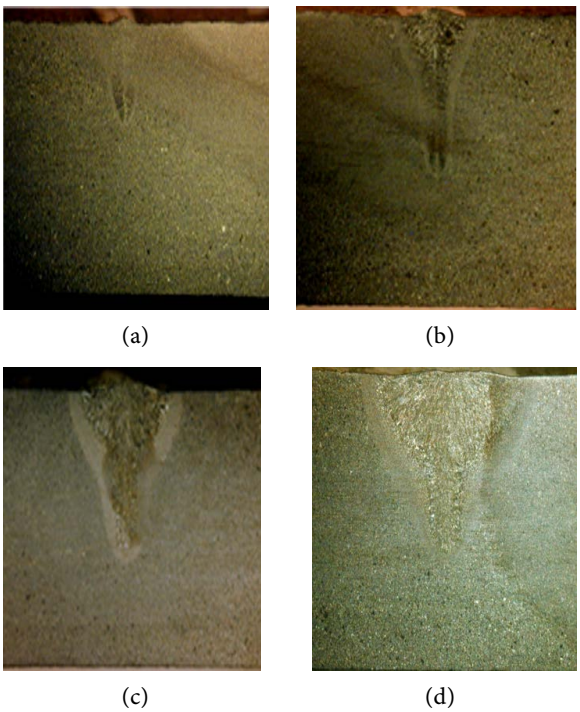

Figure 4. Macrostructure on cross-sections of the bead-on-plate welds produced on 10.0 mm thick plates of JIS G3106 SM570 by laser power of 5 kW, defocusing distance −0.5 mm, shielding gas flow rate of 30 L/min and variable welding speeds of (a) 3 m/min, (b) 2 m/min, (c) 1 m/min, (d) 0.5 m/min.

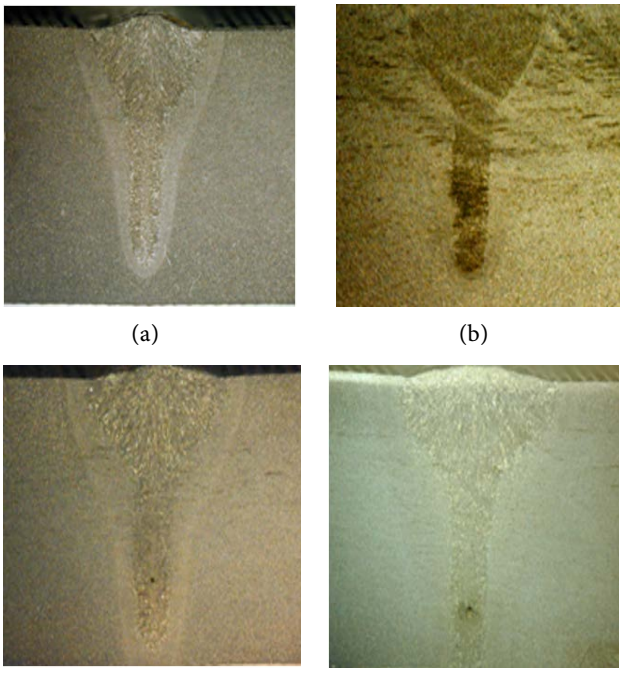

Figure 5. Macrostructure on cross-sections of the bead-on-plate welds produced on 10.0 mm thick plates of JIS G3106 SM570 by laser power of 5 kW, defocusing distance −0.5 mm, shielding gas flow rate of 30 L/min and variable welding speeds of (a) 1 m/min, (b) 0.8 m/min, (c) 0.8 m/min, (d) 0.6 m/min.

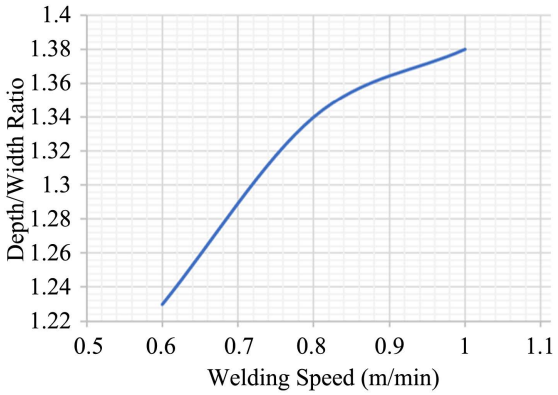

Figure 6. Influence of welding speed on weld depth/width ratio of 7 mm thickness.

Table 3. Welding parameters used for laser welding.

Power (P) (kW)	Welding Speed (S) (m/min)	Defocusing Distance (Dd) (mm)	Shielding Gas/Flow Rate (L/min)
5	0.5 - 3.0	0.0 to −1.0	Argon/15.0 - 30.0

The results showed a significant increase in the fusion zone size at lower welding speeds and consequently a decrease in depth/width ratio. Complete penetration with a relatively acceptable fusion zone size for the 7 mm base metal thickness was achieved at a welding speed of 0.6 m/min as shown in **Figure 5(d)**.

At high welding speeds, penetration is usually low because of the drop in heat input. However, in this case, the rate of increase of the weld width was significant, leading to a low depth to ratio at lower speeds although it remained within an acceptable range. The fusion zone was found to be symmetrical about the axis of the laser beam (Figure 7). The butt joint is symmetrical in shape with complete fusion. This is the expected geometry of a laser-welded joint, without excess penetration from the root side or visible porosity in the joint.

3.1.2. Effect of Defocusing Distance

The focus position, distance between the optical focal point and specimen surface, also referred to as the defocusing distance, were investigated. Figure 8 shows the face sides of the 7 mm welds made at various defocusing distances. Visual inspection of the laser-welded joints made with a defocusing distance of 0.5 mm below the specimen surface gave sound weldments with complete penetration and without defects like porosities and undercuts, Figure 9.

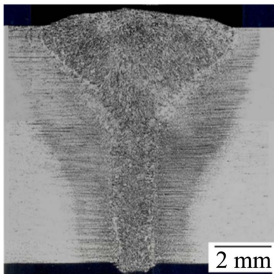

Figure 7. A cross-section of butt weld made using P = 5 kW, S = 0.5 m/min, Dd = −0.5 mm.

(a)

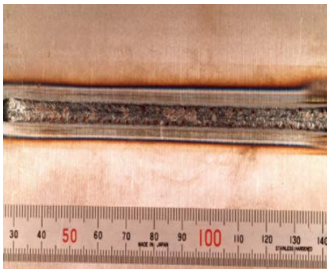

(b)

(c)

Figure 8. Face side of 7.0 mm thick plates of JIS G3106 SM570 produced by laser power of 5 kW, welding speed of 0.5 m/min, shielding gas flow rate of 30 L/min and defocusing distance (a) 0.0 mm, (b) −0.5 mm, (c) −1.0 mm.

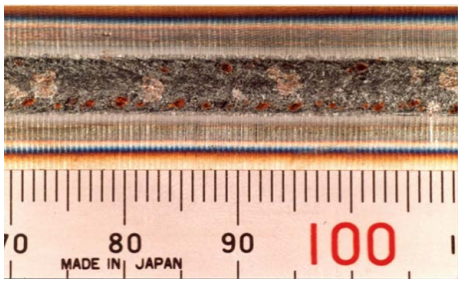

(a)

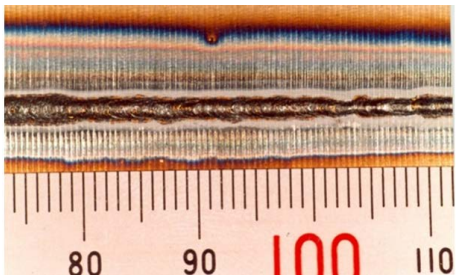

(b)

Figure 9. Butt welds of 7.0 mm thick plates of JIS G3106 SM570 produced by laser power of 5 kW, welding speed of 0.5 m/min, shielding gas flow rate of 30 L/min and defocusing distance of −0.5 mm (a) face side, (b) root side.

3.1.3. Effect of Shielding Gas Flowrate

The influence of gas shielding flow rate is determined by increasing the Argon shielding flow rate from 15 to 30 L/min at constant laser welding parameters: Laser Power of 5 kW, welding speed of 0.8 m/min and defocusing distance of −0.5 mm. Increasing the argon gas flow rate, prevented excessive plasma formation, maintained the stability of the keyhole and in turn brought about full penetration of the weld. In addition to that, at 30 L/min the cross-section of the weld was smoother with a narrower weld face and the weld root wider, **Figure 10**.

3.2. Microstructure Investigation

The base metal (BM) has a microstructure consisting of martensite and a small proportion of ferrite grains. The butt joint in this case contains identical chemical constituents to the base metal. This is because of the autogenous laser welding process in which no filler metal is used meaning the joint microstructure is also made up of martensite. Since the heat input in the HAZ was slightly below its melting point, it was sufficient enough to cause microstructural changes to give finer grains. Solidification in the weld metal (WM) led to coarse columnar grains in the microstructure (**Figure 11**).

3.3. Mechanical Properties

Figure 12 shows tensile after testing and it was observed that failure occurred by ductile rupture in the base metal. The ultimate tensile strength was 580 MPa acceptable and within the tensile strength of the base metal of 570 - 720 MPa, indicating the correctness of welding parameters, particularly laser power, defocusing

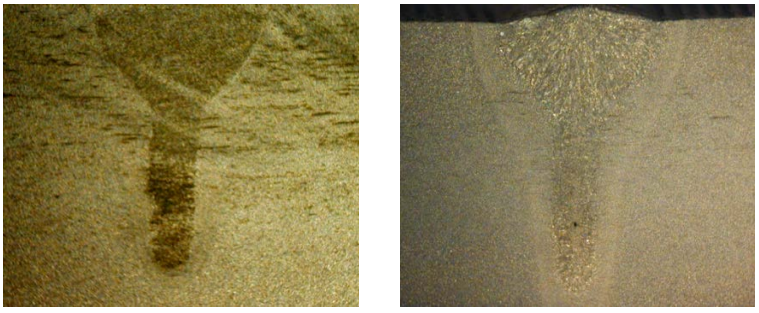

(a) (b)

Figure 10. Macrographs showing weld quality produced by laser power of 5 kW, welding speed of 0.5 m/min, a defocusing distance of −0.5 mm and a shielding gas flowrate of (a) 15 L/min, (b) 30 L/min.

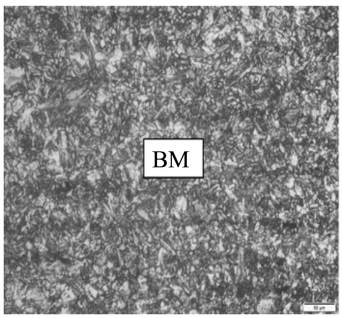

(a)

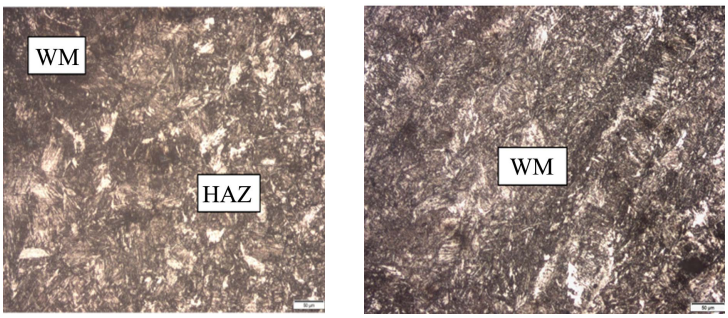

(b) (c)

Figure 11. Optical microscopic photographs at a magnification of 50 μm of the (a) used base metal used, (b) HAZ of full penetration square butt welded joint, (c) weld metal of full penetration square butt welded joint.

Figure 12. Macrographs showing fractured location in the tensile specimen.

distance, and welding speed and gas flowrate. Visual inspection also showed no structural changes which have a significant influence in decreasing mechanical properties usually brought about by the laser welding thermal cycle. Metallographic examinations also support the retaining of the material structural characteristics.

Figure 13 gives the hardness distribution of the base metal, HAZ and weld metal of JIS G3106 SM570 steel. High hardness of between 300 - 355 HV in the WM and HAZ near the weld metal. However, the least hardness of 218 HV was observed as we approach the BM. This is expected because the mechanical properties of steel, in general, are characteristic of its microstructure in these different zones. Complete penetration of 7.0 mm thickness had a width of 4.0 mm and a minimized HAZ width of 1.5 mm.

To determine the impact resistance (toughness) of JIS G3106 SM570 steel, the amount of energy absorbed during fracture was ascertained by the Charpy-V notch test. The impact toughness of the laser-welded butt joint was investigated in three different positions. The results of the Charpy-V impact toughness in the base metal (BM), HAZ and weld metal (WM) at −20˚C are shown in Figure 14. There was an uneven distribution of toughness along the butt welded joint, with the lowest impact energy observed at WM while the highest impact energy was observed in the BM. However, all measured values in all the different zones exceed the minimum required absorbed energy.

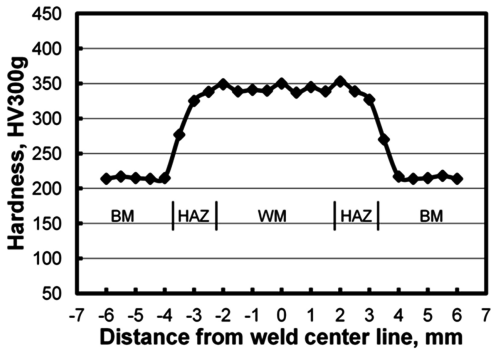

Figure 13. Hardness distribution.

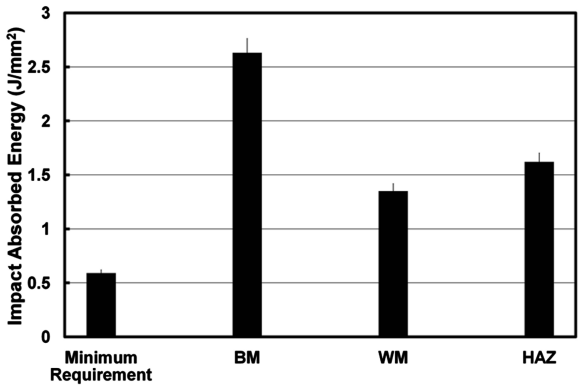

Figure 14. Impact absorbed energy distribution.

4. Conclusion

In this study, autogenous laser welding of both BOP and butt joints of JIS G3106 SM570 steel was investigated. From the study, it was found that the difficulty related to conventional fusion arc welding of high-strength quenched and tempered steel can be avoided using the non-conventional laser beam welding process. The selected optimal welding conditions were a laser power of 5.0 kW, a 500 mm/min welding speed, an argon gas shielding flow rate of 30 L/min, and a defocusing distance of −0.5 mm. An optimum butt weld with a narrow weld zone, a small heat-affected zone (HAZ), very little distortion, and a high depth-to-width ratio was made. Subjected to examination and tests, a good combination of mechanical properties including hardness (355 HV), tensile strength (580 MPa) and toughness (1.4 J/mm^2) of welded joints was observed. Laser welded joints characterised by minimum distortion as well as microstructure and mechanical properties; close to those of the base metal will enhance the application of high-strength quenched and tempered low alloy steels in bridges, ships, large-scale petroleum storage tanks, etc.

Acknowledgements

This research is funded by the Pan African University through the Institute of Basic Sciences, Technology & Innovation (PAUSTI), Kenya. The authors gratefully acknowledge the help of the Laser-X Co. Ltd.-Japan in conducting the laser welding experiments and the Central Metallurgical Research and Development Institute (CMRDI), Cairo for their support in material testing, examinations, workshops and related industrial visits. The research work is jointly supervised by both PAUSTI and CMRDI. Assistance provided by Ahmed Saiyah, CMRDI during this study is highly appreciated.

Conflicts of Interest

The authors declare no conflicts of interest regarding the publication of this paper.

References

[1] ASM International (2006) Handbook Committee, ASM Handbook, Volume 5: Heat Treatment. ASM International, Material Park, 591.

[2] Hwang, B., Lee, C.G. and Kim, S.-J. (2011) The Low-Temperature Toughening Mechanism in Thermomechanically Processed High-Strength Low-Alloy Steels. *Metallurgical and Materials Transactions A*, **42**, 717-728. https://doi.org/10.1007/s11661-010-0448-3

[3] Shaojun, S., Zeng X.P. and Sun, C.T. (2018) Heat-Treatment and Properties of High-Speed Steel Cutting Tools. *IOP Conference Series*: *Materials Science and Engineering*, **423**, Article ID: 012031. https://doi.org/10.1088/1757-899X/423/1/012031

[4] Mohrbacher, H. (2015) Guest Editorial of "Application of High Strength Steels in Lightweight Commercial Vehicles". *Advances in Manufacturing*, **3**, 1-2. https://doi.org/10.1007/s40436-015-0098-1

[5] Lange, J. and Wohlfeil, N. (2010) Examination of the Mechanical Properties of Steel S460 for Fire. *Journal of Structural Fire Engineering*, **1**, 189-204. https://doi.org/10.1260/2040-2317.1.3.189

[6] Lagneborg, R. (1991) New Steels and Steel Applications for Vehicles. *Materials & Design*, **12**, 3-14. https://doi.org/10.1016/0261-3069(91)90086-J

[7] Jindal, S., Chhibber, R. and Mehta, N.P. (2012) Issues in Welding of HSLA Steels. In: *Advanced Materials Research*, Vol. 365, Trans Tech Publications Ltd., Bäch, 44-49. https://doi.org/10.4028/www.scientific.net/AMR.365.44

[8] Gyasi, E.A. and Kah, P. (2016) Structural Integrity Analysis of the Usability of High Strength Steels (HSS). *Reviews on Advanced Materials Science*, **46**, 39-52.

[9] Lobanov, L.M., Poznyakov, V.D. and Makhnenko. O.V. (2013) Formation of Cold Cracks in Welded Joints from High-Strength Steels with 350-850 MPa Yield Strength. *The Paton Welding Journal*, **7**, 7-12.

[10] Zhao, M.S., Chiew, S.P. and Lee, C.K. (2016) Post Weld Heat Treatment for High Strength Steel Welded Connections. *Journal of Constructional Steel Research*, **122**, 167-177. https://doi.org/10.1016/j.jcsr.2016.03.015

[11] Chuvas, T.C., Garcia, P.S.P., Pardal, J.M. and Fonseca, M.D.P.C. (2015) Influence of Heat Treatment in Residual Stresses Generated in P91 Steel-Pipe Weld. *Materials Research*, **18**, 614-621. https://doi.org/10.1590/1516-1439.006315

[12] Pandey, C. and Mahapatra, M.M. (2016) Effect of Heat Treatment on Microstructure and Hot Impact Toughness of Various Zones of P91 Welded Pipes. *Journal of Materials Engineering and Performance*, **25**, 2195-2210. https://doi.org/10.1007/s11665-016-2064-x

[13] Pandey, C., Mahapatra, M.M., Kumar, P. and Saini, N. (2017) Diffusible Hydrogen Level in Deposited Metal and Their Effect on Tensile Properties and Flexural Strength of P91 Steel. *Journal of Engineering Materials and Technology*, **139**, Article ID: 031004. https://doi.org/10.1115/1.4035764

[14] Paddea, S., Francis, J.A., Paradowska, A.M., Bouchard, P.J. and Shibli, I.A. (2012) Residual Stress Distributions in a P91 Steel-Pipe Girth Weld before and after Post Weld Heat Treatment. *Materials Science and Engineering*: *A*, **534**, 663-672. https://doi.org/10.1016/j.msea.2011.12.024

[15] Landowski, M., Świerczyńska, A., Rogalski, G. and Fydrych, D. (2020) Autogenous Fiber Laser Welding of 316L Austenitic and 2304 Lean Duplex Stainless Steels. *Materials*, **13**, 2930. https://doi.org/10.3390/ma13132930

[16] Ridha Mohammed, G., Ishak, M., Ahmad, S.N.A.S. and Abdulhadi, H.A. (2017) Fiber Laser Welding of Dissimilar 2205/304 Stainless Steel Plates. *Metals*, **7**, 546. https://doi.org/10.3390/met7120546

[17] Kumar, A. and Pandey, C. (2022) Autogenous Laser-Welded Dissimilar Joint of Ferritic/Martensitic P92 Steel and Inconel 617 Alloy: Mechanism, Microstructure, and Mechanical Properties. *Archives of Civil and Mechanical Engineering*, **22**, 1-20. https://doi.org/10.1007/s43452-021-00365-6

[18] Weglowski, M.S. (2018) High Strength Quenched and Tempered Steels: Weldability and Welding. In: Branco, R., Ed., *High-Strength Steels*: *New Trends in Production and Applications*, Nova Science Publishers, Inc., Hauppauge, 143-224.

[19] Uchihara, M. and Fukui, K. (2003) Tailored Blanks of High Strength Steel-Comparison of Welding Processes. Tech. Rep., SAE Technical Paper. https://doi.org/10.4271/2003-01-2829

[20] Kang, Y., Park, G., Jeong, S. and Lee, C. (2018) Correlation between Microstructure

and Low-Temperature Impact Toughness of Simulated Reheated Zones in the Multi-Pass Weld Metal of High-Strength Steel. *Metallurgical and Materials Transactions A*, **49**, 177-186. https://doi.org/10.1007/s11661-017-4384-3

[21] Sreenivasan, N., Xia, M., Lawson, S. and Zhou, Y. (2008) Effect of Laser Welding on Formability of DP980 Steel. *Journal of Engineering Materials and Technology*, **130**, Article ID: 041004. https://doi.org/10.1115/1.2969246

[22] Steen, W.M. (2003) Background and General Applications. In: *Laser Material Processing*, Springer, London, 11-60. https://doi.org/10.1007/978-1-4471-3752-8_2

[23] Gáspár, M. (2019) Effect of Welding Heat Input on Simulated HAZ Areas in S960QL High Strength Steel. *Metals*, **9**, Article No. 1226. https://doi.org/10.3390/met9111226

[24] Njock Bayock, F., Kah, P., Layus, P. and Karkhin, V. (2019) Numerical and Experimental Investigation of the Heat Input Effect on the Mechanical Properties and Microstructure of Dissimilar Weld Joints of 690-MPa QT and TMCP Steel. *Metals*, **9**, Article No. 355. https://doi.org/10.3390/met9030355

[25] Di, H., Sun, Q., Wang, X. and Li, J. (2017) Microstructure and Properties in Dissimilar/Similar Weld Joints between DP780 and DP980 Steels Processed by Fibre Laser Welding. *Journal of Materials Science & Technology*, **33**, 1561-1571. https://doi.org/10.1016/j.jmst.2017.09.001

[26] Odebiyi, O.S., Adedayo, S.M., Tunji, L.A. and Onuorah, M.O. (2019) A Review of Weldability of Carbon Steel in Arc-Based Welding Processes. *Cogent Engineering*, **6**, Article ID: 1609180. https://doi.org/10.1080/23311916.2019.1609180

[27] El-Batahgy, A.-M., Khourshid, A.-F. and Sharef, T. (2011) Effect of Laser Beam Welding Parameters on Microstructure and Properties of Duplex Stainless Steel. *Materials Sciences and Applications*, **2**, 1443-1451. https://doi.org/10.4236/msa.2011.210195

[28] Wang, L., Xu, X.Z., Wang, K.H., Li, H. and Huang, Y. (2020) Effect of Shielding Gas and Defocusing on Porosity during Laser Beam Welding of 7A52 Alloy. *China Welding*, **29**, 20-25.

[29] Schmidt, L., Schricker, K., Bergmann, J.P. and Junger, C. (2020) Effect of Local Gas Flow in Full Penetration Laser Beam Welding with High Welding Speeds. *Applied Sciences*, **10**, 1867. https://doi.org/10.3390/app10051867

[30] Fellman, A. and Kujanpää, V. (2006) The Effect of Shielding Gas Composition on Welding Performance and Weld Properties in Hybrid CO_2 Laser-Gas Metal Arc Welding of Carbon Manganese Steel. *Journal of Laser Applications*, **18**, 12-20. https://doi.org/10.2351/1.2164481

[31] American Society for Testing and Materials (2017) Committee A-01 on Steel, Stainless Steel and Related Alloys. Standard Test Methods and Definitions for Mechanical Testing of Steel Products. ASTM International, West Conshohocken.